Laser-driven implosion of a cylindrical plasma

T. R. Clark and H. M. Milchberg
Institute for Physical Science and Technology, University of Maryland, College Park, Maryland 20742
(Received 23 October 1997)

We present what to our knowledge is the first time-resolved measurement of the electron density profile of a laser-driven concentric implosion. Cylindrically symmetric plasmas are driven by two spatially coincident line-focused laser pulses. If a plasma channel is allowed to form after the first pulse, the second pulse drives an inward compression wave which converges on the channel axis and later relaxes. The two-pulse absorption and ionization can significantly exceed that due to a single pulse of the same total energy, with the second pulse being almost totally absorbed. [S1063-651X(98)08603-6]

PACS number(s): 52.40.Nk, 52.35.Mw, 52.40.Db

INTRODUCTION

Laser-heated, thermally driven plasma channels are a new means for controlling intense laser-matter interactions [1]. One of the striking features of these channels is their high degree of radial and axial symmetry [2], which results from using axicon or conical lens focusing optics [3,4] for the generation of the plasma in a uniform density gas backfill. With the conical wave produced by an axicon, optical rays approach the focus from the side, with the important consequence that the laser energy responsible for elongated plasma generation and heating passes through little intervening plasma [3]. For pulses shorter than $\sim 100-200$ ps, little radial plasma motion on a scale comparable to the heated region's diameter takes place during the pulse. Pulses which are too short would tend to transfer and amplify nonuniformities in the laser beam profile onto the axial electron density profile, with little opportunity for smoothing by electron thermal diffusion and collisional ionization during the pulse. A longer pulse can continue to heat the plasma while such electron density nonuniformity is smoothed. The 100-ps pulses used in these experiments are appropriate for subatmospheric density range gas targets, since they are comparable to or shorter than the fastest hydrodynamic time scale of shock wave evolution, and they are sufficiently long for thermal smoothing to eliminate density nonuniformity [3].

The plasma columns resulting from axicon-focused short laser pulses therefore make possible the investigation of laser-driven plasma hydrodynamics in a highly symmetric, one-dimensional regime. This is of interest for benchmarking of codes modeling laser-plasma interactions [5], basic studies of high temperature shock phenomena in laboratory and astrophysical plasmas [6], and applications such as the control of guided optical modes [7].

In this paper we present measurements of the dynamics of a cylindrically symmetric laser plasma driven by two spatially coincident laser pulses of variable temporal separation focused in an ambient gas. We find that the resulting hydrodynamic evolution depends significantly on the energy ratio and delay between the two pulses. If the second pulse is applied after a characteristic time determined by plasma expansion, the resulting total absorption and ionization significantly exceeds that obtained by a single pulse of the same total energy, with the second pulse almost totally absorbed. For delays long enough to allow a plasma channel to form after the first pulse, the second pulse drives an inward compression wave, resulting in a significant on-axis density enhancement. In previous work [7], we showed that the application of a second axicon pulse to an already developed channel would result in the cutoff of guiding of a probe pulse injected at the channel entrance after ~ 1-ns delay, followed by the appearance of an annular mode at further delay, and eventually a return to a central mode. We attributed these effects to a compression wave driven by the second heating pulse. This has now been verified experimentally.

In recent work of other groups, soft x-ray interferometry was used to measure electron density profiles in colliding plasmas from segmented solid targets [8], and x-ray backlighting [9] and spectral line analysis [10] has made possible the inference of mass density and electron density in the much higher density environment of imploded inertial confinement fusion capsules. But to our knowledge, our experiment is the first *direct* measurement of the time-resolved electron density profile of a laser-driven concentric implosion.

EXPERIMENTAL SETUP

The laser used in this experiment is a mode-locked Nd:YAG (yttrium aluminum garnet) oscillator–regenerative and power amplifier system. Two spatially coincident output pulses with adjustable relative energy and delay were produced by injecting the regenerative amplifier with two seed pulses, ensuring collinearity throughout the rest of the optical system. This was essential to achieving spatial overlap and plasma compression symmetry over the full extent of the axicon line focus. The relative intensity and delay between the two pulses was controlled at the regenerative amplifier input by a half wave plate plus polarizing beam splitter and an optical delay line (0–6 ns). The two output pulses (1.064 μm, 100 ps, total energy ~ 500 mJ) generated and heated the plasma at the ~ 1-cm-long line focus of a 35° base angle axicon, with peak intensity 5×10^{13} W/cm^2.

Figure 1 shows the optical arrangement for plasma generation and heating, and for electron density measurement. Time- and space-resolved density profiles were determined using a folded wave front interferometer [2], where the 532-nm, 100-μJ, 70-ps interferometer probe pulse was obtained

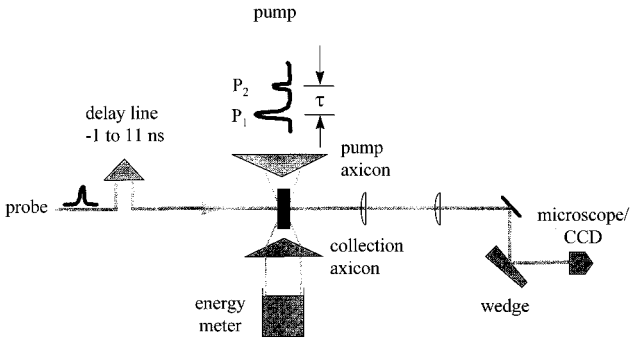

FIG. 1. Optical arrangement, showing pump pulses P_1 and P_2 (1064 nm, 100 ps) with separation τ passing through the pump axicon, the collection axicon for absorption measurement, and the folded wave front interferometer with probe pulse (532 nm, 70 ps), imaging optics (shown schematically) and reflection wedge. The plasma is shown between the pump and collection axicons.

by frequency doubling a portion of the 1064-nm light split off at an earlier point in the Nd:YAG system amplifier chain. The ratio between the two 1064-nm pump pulses, P_1 and P_2, was sufficiently large that the interferograms were dominated by a single 532-nm probe pulse. The probe was passed through an optical delay line with delay of -1 to 11 ns with respect to the first pump pulse. Single shot interferograms were recorded on a charge coupled device camera and digitized by a frame grabber. The spatial resolution of the system was set by the overall magnification of $\sim 25\times$ to be $\sim 1.5\ \mu$m/pixel, while the temporal resolution of 70 ps was set by the probe pulse duration. Pump absorption measurements were made by using a second, large aperture axicon to recollimate laser energy passing through the pump axicon focus, and directing it to an energy meter. Fresnel reflection from the channel wall, scattering, and off-resonant side coupling to channel modes [11] are all small so that the reduction in pump energy transmitted through the focus was attributed to absorption.

EXPERIMENTAL RESULTS AND DISCUSSION

Figure 2 shows fractional absorption of the total energy as a function of delay between the two pump pulses (the first pulse to second pulse energy ratio was $\sim$2.7:1) for a 180 torr Ar–20 torr N_2O gas mixture. This energy ratio allowed ionization by the first pulse to neonlike Ar on axis, making the analysis more straightforward as will be seen below. The N_2O component field-ionizes early in the pulse at $\sim 10^{13}$ W/cm^2 and provides seed electrons for the uniform avalanche breakdown of Ar [2]. In the range of delay 0.5–5 ns, the total absorption of the two pulses increased by almost a factor of 6. The gap in the plot between 3 and 5 ns is due to blocking of the regenerative amplifier injection beam path by the delay line translator. The inset shows fractional absorption of the second pulse alone, indicating greater than 90% absorption at 5-ns delay, a value as high as absorption in long scale length plasmas from solid targets [12] or in clusters produced by supersonic nozzles [13].

The dynamics of this absorption process and the subsequent plasma evolution are shown in the time-resolved elec-

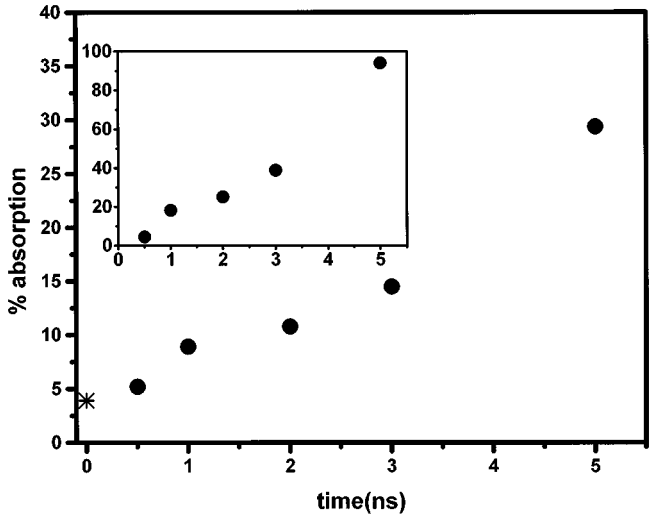

FIG. 2. Percent absorption vs delay between the two pump pulses for first pulse to second pulse energy ratio 2.7:1. The point at zero delay is for absorption of a single 500-mJ pulse. The inset is a plot of absorption of the second pulse 135 mJ alone, calculated using the known absorption of first 365-mJ pulse. The gas mixture is 180-torr Ar–20-torr N_2O.

tron density profiles of Fig. 3 for the 2.7:1 energy ratio of Fig. 2 and a two-pulse delay of 1.5 ns. Channel formation occurs within a few hundred picoseconds of the first pulse, as seen in Fig. 3(a). By 1.9 ns, or within $\sim$400 ps after the second pulse, the electron density at the outer side of the shock region has grown significantly. It is at this time that a prompt increase in guided light transmission in a low order mode was observed [7], and this can now be clearly attributed to the enhanced channel wall. By $\sim$0.5 ns after the application of the second pulse, the shock region has split [Fig. 3(b)], with the appearance of an inwardly directed compression wave along with the continuing outward shock propagation, which is newly accelerated. During this phase, guiding of low order modes was observed to be cut off [7]. The compression wave, moving at an average velocity of 5×10^6 cm/s, reaches the channel axis $\sim$1.5 ns after the second pulse, and the electron density peaks another nanosecond later [Fig. 3(c)], at a level higher than in the shock and approaching the level reached immediately after the first pulse. Around this delay time, guiding was observed to occur in annular modes [7]. The central peak then relaxes over the next $\sim$2 ns as the density returns to the typical channel profile produced by a single pulse. During this period, the annular guided mode was observed to fill in and a central mode reappeared [7]. For pump pulse separations of less than $\sim$1 ns at this gas fill pressure, a compression wave was not observed because sufficiently deep channel formation (or a distinct channel wall) did not have time to develop in advance of the second pulse.

To understand these dynamics, a model calculation was performed for 200 torr Ar irradiated by two 100-ps full width at half maximum pulses separated by 1.5 ns, with a peak intensity ratio of 2.7:1 and first pulse peak intensity of 7×10^{13} W/cm^2. A J_0 profile (zero order Bessel beam), with radius to first zero of $\sim 3\ \mu$m, was used to model the axicon focus. The model is a one-dimensional (in radial coordinate) Lagrangian hydrocode [1], which includes field ionization

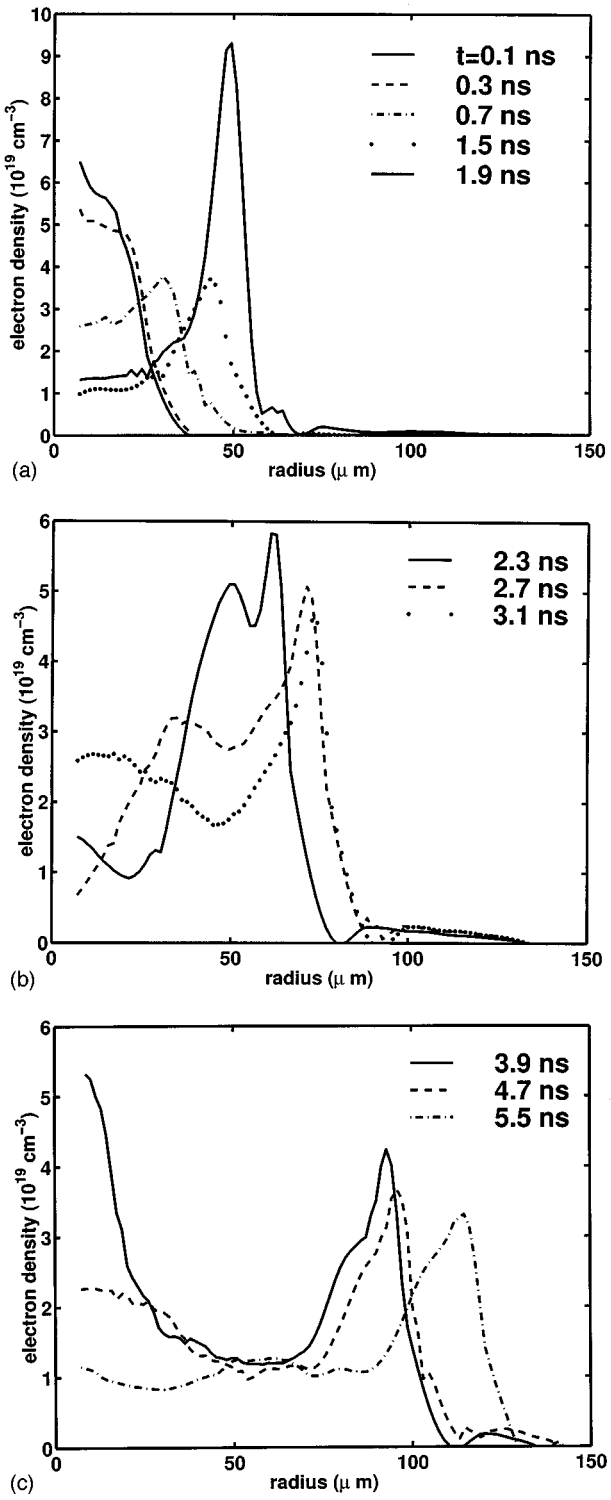

FIG. 3. (a), (b), and (c) Measured electron density profiles for two-pulse irradiation. Times shown for the probe pulse are relative to the arrival of the first pump pulse ($t=0$). The second pump pulse arrives at $t=1.5$ ns.

[14], inverse bremsstrahlung heating, thermal conduction (taken to be the lesser of the gradient based flow or the flux-limited flow at each grid point), collision-based ionization and recombination, and collisional energy exchange between electrons and ions. The peak intensity used in the calculation was higher than the measured vacuum value of 5×10^{13} W/cm^2 in order to achieve peak ionization on an axis similar to that measured in the experiment. In this context, we note that at present our hydrocode calculation does not consider the effect of the plasma on the laser field. Figure 4(a) shows the pressure profiles $P(r)$ just before (1.5 ns) and after (1.7 ns) the second pulse arrives (the peak pulse intensity of the second pulse occurs at $t=1.62$ ns in the calculation). Just to the left of the peak pressure in the 1.7-ns curve, the force per unit volume on the plasma, $-\partial P/\partial r$, points inward, and just to the right of the peak $-\partial P/\partial r$ points outward. It is therefore clear that the compression wave and the newly accelerated outward shock are driven by strongly enhanced inward and outward forces from the pressure gradients produced through heating and ionization by the second pulse in the cool dense plasma of the original shock region. The subsequent evolution of the electron density profile to maximum compression is shown in Figs. 4(b) and 4(c), which show qualitative agreement with the measurements of Fig. 3.

The time-resolved electron density profiles were used to extract estimates of the post-pulse temperature evolution. Figure 5 shows the shock position (taken to be the half maximum phase shift point on the interferogram [2]) vs time for a single pulse [Fig. 5(a)], and for two-pulse cases (energy ratio 2.7:1) of the same total energy with pulse separations of 500 ps [Fig. 5(b)] and 1.5 ns [Fig. 5(c)]. In the two-pulse cases, the outgoing shock position was used for these plots. Least squares fits were made to the expression $R_s=\alpha t^m$ for the shock radial position, giving $m=0.5$ to within 10%, with α depending on the plot and segment. For the 1.5-ns separation, there is a distinct break in the shock evolution after the second pulse arrives (consistent with the extra velocity kick imparted by the second pulse) so that two best fit segments are shown for this plot. A break could not be discerned in the 500-ps delay data, since an initial shock had not yet clearly formed. An exponent m close to $\frac{1}{2}$ identifies the dynamics as nearly adiabatic expansion of a cylindrical blast wave for which the self-similar solution [15] gives $\alpha=\xi_0(E/\rho_0)^{1/4}$, where E is the initial energy per unit length of cylinder available to drive the expansion, ρ_0 is the initial mass density, and ξ_0 is a dimensionless factor of order unity which depends on the specific heat ratio [16]. In both single- and double-pulse measurements at various energy ratios, delays, and gas fill pressures, we find consistently that $m\approx0.5$, corresponding to nearly adiabatic expansion of the plasma. The hydrocode calculations support this interpretation. In our previous work we argued that in single-pulse channel generation, rapid conduction cooling dominates within the first few hundred picoseconds of a driving pulse, and adiabatic expansion dominates thereafter [2]. Figure 6 shows the shock velocities, taken as the derivatives of the fitting curves in Fig. 5. The effect of the second pulse is to increase the outward shock speed, with the abruptness of this increase clearly seen in the 1.5-ns result. It is notable that the average inward compression wave speed quoted above, 5×10^6 cm/s, considerably exceeds any of the outward shock speeds plotted here.

Temperature estimates can be made by setting the measured outward shock speed equal to the approximate shock speed $c_s\sim\sqrt{ZkT_e/m_i}$, ignoring in this expression a factor of order unity which is a function the specific heat ratio [15].

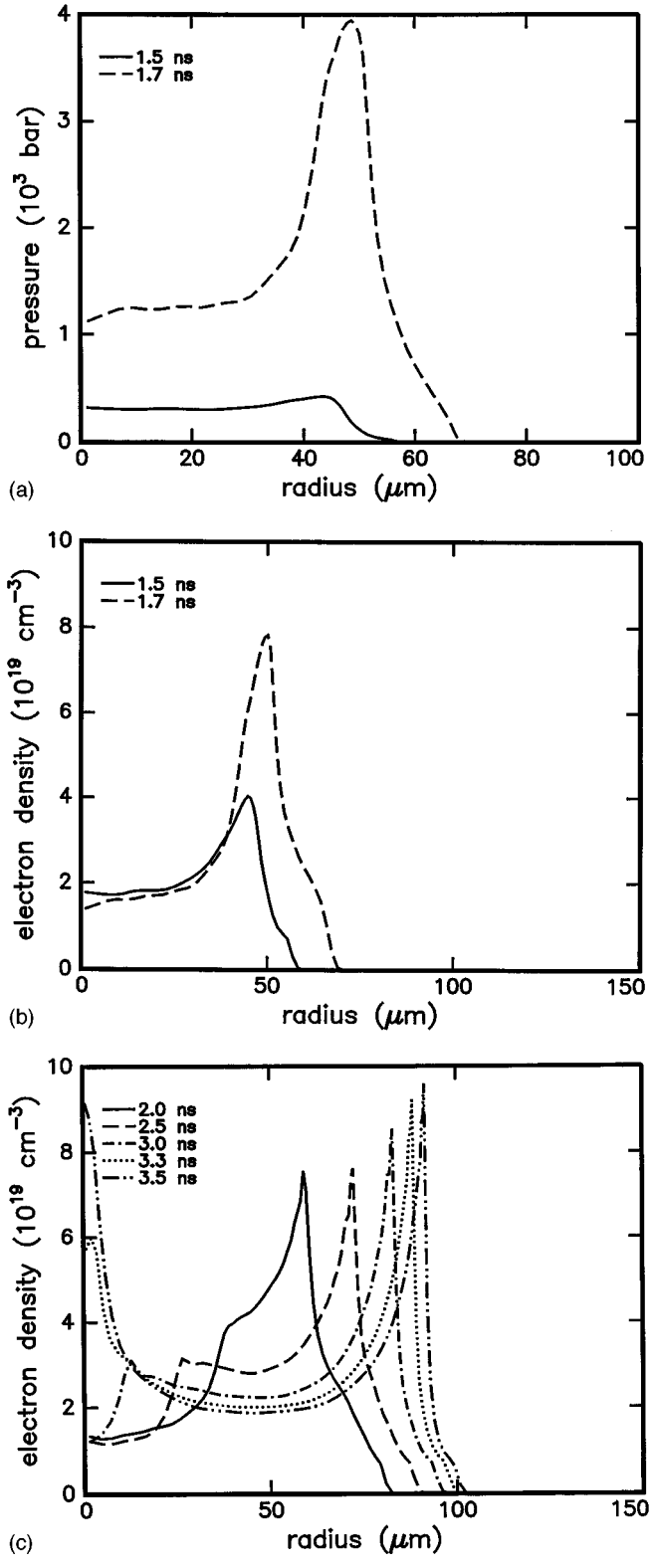

FIG. 4. (a) Calculated pressure profiles just before (1.5 ns) and after (1.7 ns) the second pump pulse, which peaks at $t=t_2=1.62$ ns. Calculated electron density profiles (b) just before and after the second pulse, and (c) during the phase of the compression wave. Parameters: first pulse intensity 7×10^{13} W/cm^2; second pulse intensity 2.5×10^{13} W/cm^2, 200-torr Ar; the laser field profile is J_0, with the first zero at 3-μm radius.

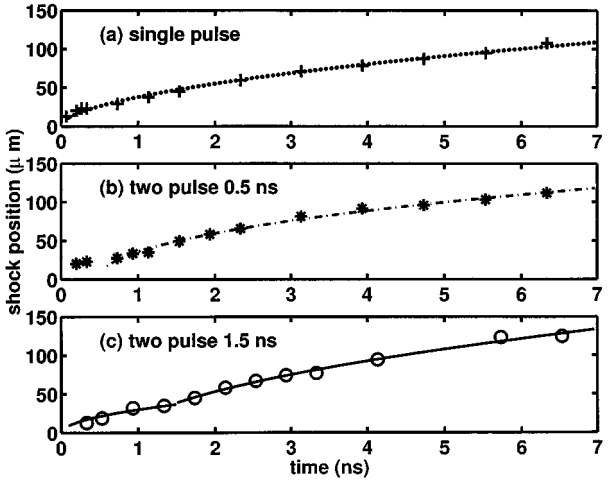

FIG. 5. Outward-moving shock radius vs time for (a) a single pulse; (b) two-pulse, 500-ps separation; and (c) two-pulse, 1.5-ns separation.

Here $\overline{Z}=N_e/\Sigma_i N_i$ is the measured peak average ionization on axis, where N_e is the electron density and N_i is the density of ion species i, T_e is the on-axis temperature, m_i is the ion mass, and k is Boltzmann's constant. Using our hydrocode, we have verified that the above expression for c_s agrees to within $\sim$20% of the simulation's shock speed over a wide range of conditions once shock motion has begun (or has changed) within a few hundred picoseconds of the first (or second) pulse. Figure 7 shows this comparison for the calculation parameters of Fig. 4, and provides confidence for use of the measured shock speed as a temperature diagnostic. For the case of a single pulse, temperature estimates are particularly straightforward since peak $\overline{Z}$ remains approximately constant for many nanoseconds after the initial ionization. Therefore, early time values $\overline{Z}\approx[N_e(r=0,t<200\ \text{ps})]/[\Sigma_i N_i(r=0,t<200\ \text{ps})]$ can be used at later times, where $\Sigma_i N_i(r=0,t<200\ \text{ps})\approx N_0$, the neutral atom density in the gas backfill [2]. At times greater than $\sim$200 ps after the pulse, enough mass density reduction occurs on axis due to the cylindrical expansion that N_0 is not a good measure of

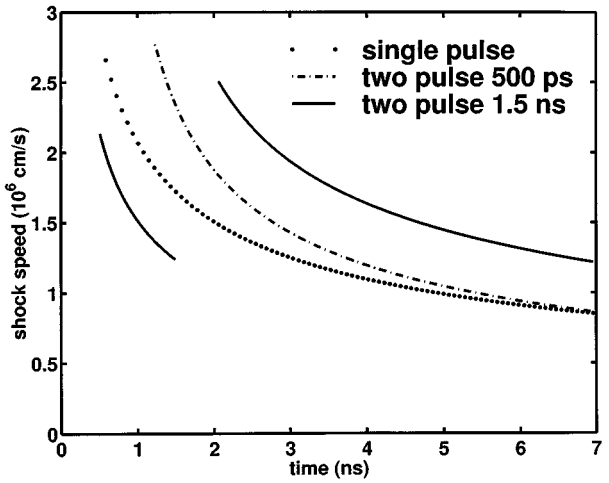

FIG. 6. Outward-moving shock speed, taken as the derivative of the fits to Figs. 5(a), 5(b), and 5(c).

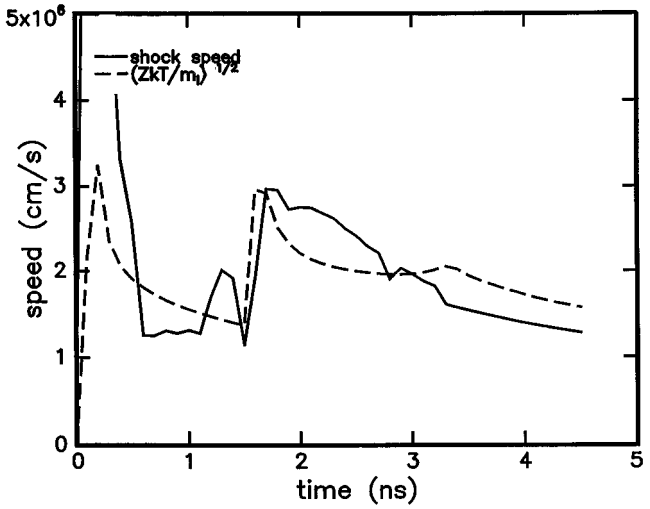

FIG. 7. From the hydrocode: comparison of the shock speed (time derivative of peak density position in outward-going shock) to the expression $c_s=\sqrt{ZkT_e/m_i}$.

the sum of the ion densities. For the single-pulse case, the peak ionization at early times was determined from interferometry to be $Z\approx 7$. For the two-pulse cases (energy ratio 2.7:1 with 500-ps and 1.5-ns delays), $Z\approx 7$ was determined after the first pulse alone. The second pulse in each case does not significantly change the on-axis electron density or Z [see Fig. 3(a), where the main effect of the second pulse is ionization at the channel periphery]. Assuming ionization to the He-like states of N and O gives $Z_{\text{argon}}\approx 8$, the robust neonlike state (the ionization potential is equal to 422 eV). It is therefore not surprising that the second pulse does not change Z on axis. For our conditions, constant $Z\approx 7$ was therefore used for the temperature estimation in all three cases.

Figure 8 is a plot of the approximate on-axis plasma temperatures, where, for the two-pulse cases, the long time temperature asymptotes remain higher than the single-pulse asymptote, evidence that they are higher energy adiabats,

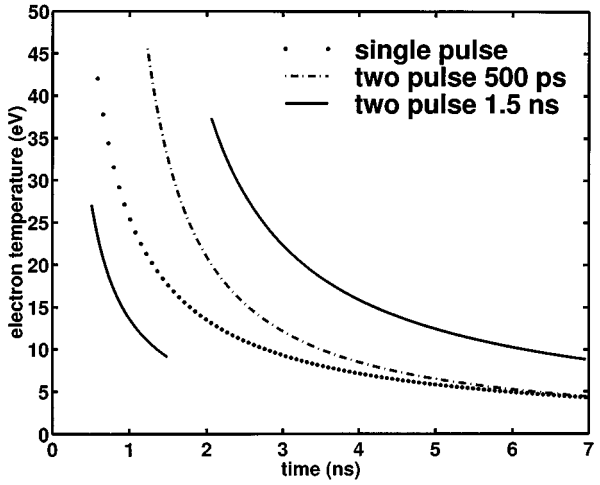

FIG. 8. Estimated on-axis temperatures, from setting the shock speeds of Fig. 6 equal to $\sqrt{ZkT_e/m_i}$, where Z is determined from interferometry.

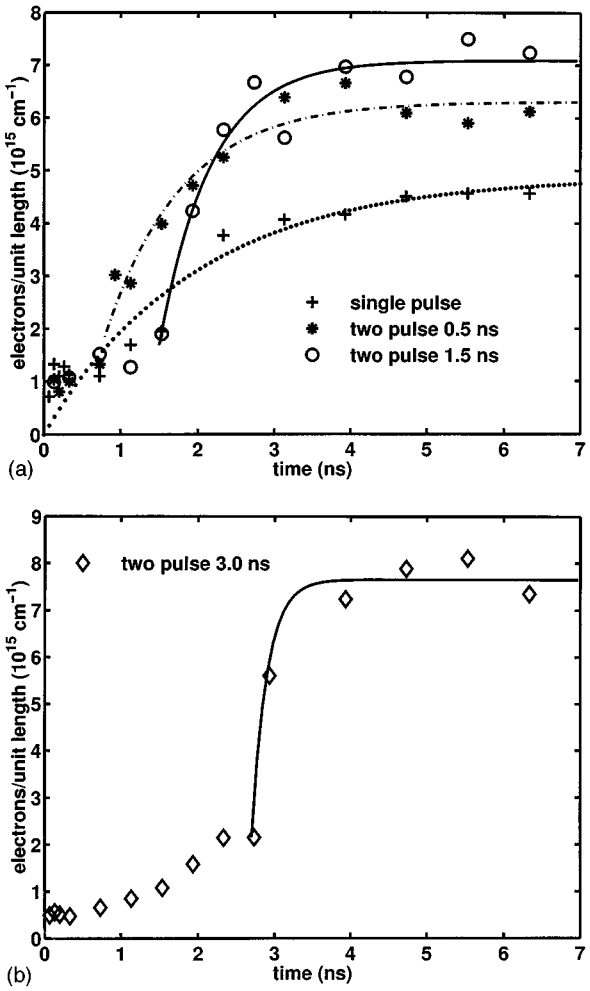

FIG. 9. (a) Number of electrons per unit length of a channel for single-pulse and two-pulse cases (first pulse to second pulse energy ratio 2.7:1, with pulse separations of 500 ps and 1.5 ns). (b) First pulse to second pulse energy ratio 2:1, and pulse separation 3.0 ns. Total energy 500 mJ.

arising because the long time dynamics for the two-pulse case scales as if more total energy per unit mass density E/ρ_0 were absorbed at early times. These temperatures and the measured electron density profiles are consistent with the absorption measurement of Fig. 2: a simple calculation of inverse bremsstrahlung absorption coefficients using the measured density and temperature gives absorption in reasonable agreement with the data.

The radial integral of the experimental electron density profiles provides further insight into the absorption and ionization dynamics in these cylindrical plasmas. In Fig. 9(a) we show the number of electrons per unit length of channel [$Q=\int_0^{R_s+\Delta R_s} N_e(r)2\pi r\,dr$, where R_s is the shock radial position and ΔR_s is the approximate shock width] for the three cases discussed above. The points are fitted to the heuristic expression $Q=Q_0+\Delta Q(1-e^{-t/\tau})$, where τ is a time scale for ionization increase. The total ionization is enhanced in the two-pulse driven plasmas, and τ in all cases is greater than the laser pulse width of 100 ps. Inspection of the density profiles shows that beyond a few hundred picoseconds the continuing growth in the ionization originates near the plasma edge. The fits give $\tau=2.0$ ns for the single-pulse

case, and 1.0 and 0.7 ns, respectively, for the 500-ps and 1.5-ns pulse separations. For a 3-ns pulse separation and 2:1 energy ratio, $\tau = 0.2$ ns, as shown in Fig. 9(b). This dramatic reduction in τ with increased pulse separation (and increased shock radius R_s) is clearly understood by considering the scaling with R_s of the rate of increase of charge, $dQ/dt = (d/dt)\int_0^{R_s(t)+\Delta R_s} N_e(r,t) 2\pi r\, dr \approx 2\pi R_s [c_s N_{es} + \Delta R_s \times (\partial N_{es}/\partial t)]$, where N_{es} is the peak density at the shock. This effect reemphasizes that the excess ionization induced by the second pulse occurs mainly at the plasma periphery, at least under the conditions explored here. As a result, not only is the reduction of temperature with delay important in the enhanced absorption, but so is the larger surface area (containing the high density plasma of the shock) presented by the expanded channel to a second pulse.

CONCLUSIONS

Measurements of the hydrodynamics of a cylindrically symmetric two-pulse excited cylindrical laser plasma have been presented. The total energy absorption and ionization is found to be enhanced when a portion of the laser energy is applied after the plasma created by the first pulse has expanded and cooled. The shock region of the channel presents a dense, cool, and large surface area plasma for efficient absorption of the second pulse, and the absorption can be as high as in long scale length plasma from a solid target or in cluster target plasmas. The high degree of symmetry and efficiency of this absorption makes possible the generation of laser-driven concentric implosions, which were measured for the first time, to our knowledge, with time-resolved interferometry.

ACKNOWLEDGMENTS

We acknowledge support by the National Science Foundation (Grant No. PHY-9515509) and the AFOSR (Grant No. F49620-96-10095).

[1] H. M. Milchberg, T. R. Clark, C. G. Durfee, T. M. Antonsen, and P. Mora, Phys. Plasmas **3**, 2149 (1996).
[2] T. R. Clark and H. M. Milchberg, Phys. Rev. Lett. **78**, 2373 (1997).
[3] C. G. Durfee, J. Lynch, and H. M. Milchberg, Phys. Rev. E **51**, 2368 (1995).
[4] O. G. Ivanov, R. I. Okunev, L. N. Pakhomov, V. Yu. Petrun'kin, L. Ya. Polonsky, and L. N. Pyatnitsky, Zh. Tekh. Fiz. **32**, 1212 (1987) [Sov. Phys. Tech. Phys. **32**, 1212 (1987)].
[5] G. B. Zimmerman and W. L. Kruer, Comments Plasma Phys. Control. Fusion **2**, 51 (1975).
[6] J. Grun, J. Stamper, C. Manka, J. Resnick, R. Burris, J. Crawford, and B. H. Ripin, Phys. Rev. Lett. **66**, 2738 (1991); W. I. Newman, Astrophys. J. **236**, 880 (1980); E. T. Vishniac, *ibid.* **274**, 152 (1983).
[7] C. G. Durfee, T. R. Clark, and H. M. Milchberg, J. Opt. Soc. Am. B **13**, 59 (1996).
[8] D. H. Kalantar, S. W. Haan, B. A. Hammel, C. J. Keane, O. L. Landen, and D. H. Munro, Rev. Sci. Instrum. **68**, 814 (1997).
[9] A. S. Wan, T. W. Barbee, R. Cauble, P. Celliers, L. B. Da Silva, J. C. Moreno, P. W. Rambo, G. F. Stone, J. E. Trebes, and F. Weber, Phys. Rev. E **55**, 6293 (1997).
[10] N. C. Woolsey, B. A. Hammel, C. J. Keane, A. Asfaw, C. A. Back, J. C. Moreno, J. K. Nash, A. Calisti, C. Mossé, R. Stamm, B. Talin, L. Klein, and R. W. Lee, Phys. Rev. E **56**, 2314 (1997).
[11] T. R. Clark and H. M. Milchberg (unpublished).
[12] C. E. Max, in *Laser-Plasma Interaction*, edited by R. Balian and J. C. Adam (North Holland, Amsterdam, 1982), p. 301.
[13] T. Ditmire *et al.*, Phys. Rev. Lett. **78**, 3121 (1997); K. Kondo *et al.*, J. Phys. B **30**, 2707 (1997).
[14] M. V. Ammosov, N. B. Delone, and V. P. Krainov, Sov. Phys. JETP **64**, 1191 (1986).
[15] L. Sedov, *Similarity and Dimensional Methods in Mechanics* (Academic, New York, 1959).
[16] Ya. B. Zeldovich and Yu. P. Raizer, *Physics of Shock Waves and High Temperature Hydrodynamic Phenomena* (Academic, New York, 1966).